Proceedings of the ASME 2014 12th International Conference on Nanochannels, Microchannels, and Minichannels
ICNMM2014
August 3-7, 2014, Chicago, Illinois, USA

ICNMM2014-21779

MIXING AND HEAT TRANSFER IN HELICAL CAPILLARY FLOW REACTORS WITH ALTERNATING BENDS

Marius G. Gelhausen
TU Dortmund University, Biochemical and Chemical Engineering, Laboratory of Chemical Reaction Engineering
Emil-Figge-Str. 66, 44227 Dortmund, Germany

Safa Kutup Kurt, Norbert Kockmann
TU Dortmund University, Biochemical and Chemical Engineering, Laboratory of Equipment Design
Emil-Figge-Str. 68, 44227 Dortmund, Germany

ABSTRACT

Capillary flow is often occurring in natural and technical systems. Due to small diameter channels, laminar flow is established, while heat transfer is high from large specific surface area. For chemical reactions, good mixing and a narrow residence time distribution are important for high selectivity and yield. To improve mixing and residence time distribution, several measures of bend flow, helical arrangements and curved capillaries are proposed in literature. This contribution describes the flow, residence time distribution, and its influence on chemical reactions in short helical, alternating reactor capillaries (SHARC). The influence of the number of bends between alternating coils on the residence time distribution is described for different capillary and coil diameter, coil length and flow rate in laminar regime. The residence time distribution is a good measure for axial mixing and dispersion, while the heat transfer is mainly affected by the flow rate. The SHARC device was built from polymer capillaries of fluorinated ethylene propylene (FEP, inner diameter of 0.38 and 0.75 mm) with high mechanical flexibility for bending and good chemical resistance. Despite of low heat conductivity of the wall material, volumetric heat transfer coefficients of more than 5 MW/m^3K were measured in a water bath. A highly exothermic reaction with adiabatic temperature increase of more than 100 K could be operated without detecting reaction runaway.

INTRODUCTION

The temperature control of a reactor in a process design is a fundamental issue, which strongly influences the performance in terms of conversion, selectivity and process safety [1]. In general, intensified processes offer additional process safety. Tubular reactors with micro scale dimensions are especially suitable because they have a higher surface to volume ratio than macro scale reactors. This enhances heat transfer and minimizes liquid hold up. Easy scale up and high production flexibility to market demands are further advantages and allow for short time to market of new products [2]. However, low Reynolds numbers increase dispersion due to a laminar flow profile, which limits the reactor performance [3]. Helically coiled tubes can overcome heat and mass transfer limitations by inducing secondary flow due to centrifugal forces. This leads to homogeneous temperature profiles and reduced axial dispersion [4] [5]. But after the flow profile is developed, the cross section is divided in two separate zones by Dean vortices. Furthermore, fluid elements tend to stay on the same flow paths and do not mix. Fluid compartments inside the Dean vortex are not in contact with the wall for heat exchange [6]. The reactor type named “coiled flow inverter” (CFI) was developed to overcome these drawbacks [7] [8]. It consists of a coiled tube, where the

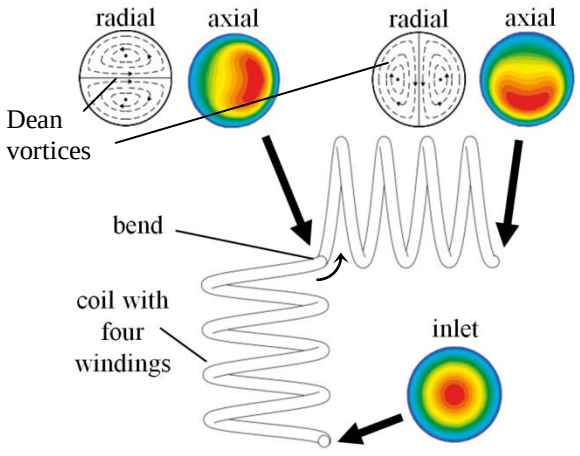

Figure 1: Schematic of radial flow profiles at different positions in a CFI. Dean vortices occur in radial direction [8].

coil direction and thus the direction of centrifugal force acting on the fluid elements is changed by bends (see Figure 1).
After each bend, the fluid elements follow chaotic trajectories because of the altered direction of the centrifugal force. After a certain development length, the typical flow profile with Dean vortices is rebuilt again. In a short helical alternating reactor capillary (SHARC), the fraction of parts with chaotic fluid trajectories is kept high by an increasing number of bends between the coils. Yet the bends increase pressure drop in the range of $25 \leq Re \leq 1200$ by about 5% compared to helically coiled tubes. A higher stability of laminar flow has also been ascertained [7].
Two forces contribute to the Dean vortex formation: centrifugal and torsion force. The occurrence of secondary flow depends on the Dean number *Dn* with d_i being the inner tube diameter, D_{coil} the coil diameter and *Re* the Reynolds number [9].

$$Dn = \frac{\rho u d_i}{\eta}\sqrt{\frac{d_i}{D_{coil}}} = Re\sqrt{\frac{d_i}{D_{coil}}} \tag{1}$$

For *Dn* > 3, Dean vortices were found to occur under the assumption of a torus [10]. When a finite pitch of a coil is regarded, the Dean number is extended to the Helical number *He* with *h* being the pitch and δ the curvature [9].

$$He = Re\sqrt{\delta} = Re\sqrt{\left(\frac{\frac{D_{coil}}{2}}{\frac{D_{coil}{}^2}{4} + \left(\frac{h}{2\pi}\right)^2}\right)} \tag{2}$$

Finite pitch leads to torsion, which alters the laminar flow profiles and decreases the radial vortex intensity. To characterize this effect, the torsion number η_{coil} and the Germano number *Gn* are introduced [11].

$$\eta_{coil} = \frac{\frac{h}{2\pi}}{\frac{D_{coil}{}^2}{4} + \left(\frac{h}{2\pi}\right)^2} \tag{3}$$

$$Gn = Re \cdot \eta_{coil} \tag{4}$$

It was mathematically shown that the ratio of centrifugal to torsion force can characterize, which radial secondary flow profile occurs. This is done by the helical flow group ς.

$$\varsigma = \frac{Gn}{He^{3/2}} < 0.2\, m^{-0.25} \tag{5}$$

Please note that the unit of ς is $m^{-0.25}$. For values of $\varsigma < 0.2\, m^{-0.25}$ the secondary flow consists of two vortices, for higher values only one occurs. This is not favorable as the intensity of radial mixing is smaller for one vortex [9] [11].
In this paper, the SHARC reactor design is described with two different designs. They are assessed in terms of residence time distribution (RTD) and heat transfer characteristics. The fast and highly exothermic oxidation of sodium thiosulfate (TS) and hydrogen peroxide (HP) was carried out in both reactors. The SHARC reactor was suitable to handle high adiabatic temperature rises and, therefore, high reaction heat. Furthermore, the SHARC design shows narrow RTD with high Bodenstein numbers due to low axial dispersion.

SHARC DESIGN

The narrowest RTD is obtained for 90° bends as this causes a complete flow inversion [10]. In general, the number of bends needs to be maximized for the narrowest RTD, because it is the most influential factor on the RTD performance [10] [12]. This implies also that the number of coil windings have to be minimal for introducing chaotic flow paths and Dean vortices. It is therefore necessary to determine the number of coils, after which the flow profile is developed. A length in a torus can be calculated depending on coil diameter and the number of windings. Explicit equations for correlations of $n_{winding}$ and D_{coil} for helically coiled tubes and CFIs can be found for various cases in literature and are stated below [13] [14] [15] [16]. The correlation between those for an inner tube diameter of 0.75 mm is shown in Figure 2.

$$\frac{Re \cdot Sc}{1300\pi}\left(\frac{d_i}{D_{coil}}\right) > n_{winding} \tag{6}$$

$$n_{winding} = \frac{2}{\pi}(2Re)^{\frac{1}{2}}\left(\frac{d_i}{D_{coil}}\right)^{\frac{3}{4}} \tag{7}$$

$$n_{winding} = \frac{49°}{360°}Re^{\frac{1}{3}}\left(\frac{d_i}{D_{coil}}\right)^{\frac{1}{2}} \tag{8}$$

$$\frac{25}{\pi}\left(\frac{d_i}{D_{coil}}\right) > n_{winding} \tag{9}$$

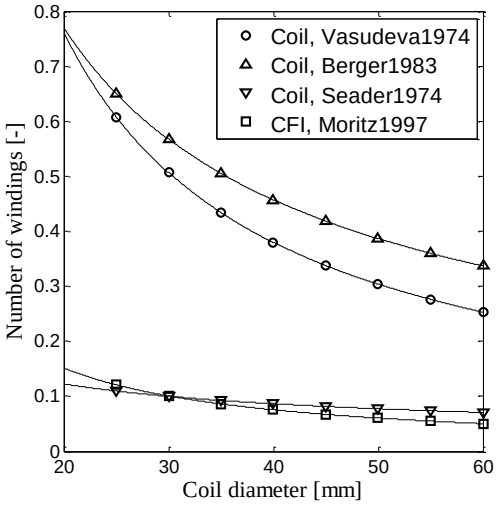

Figure 2: Calculated entry lengths for number of coils depending on the coil diameter. An inner tube diameter of 0.75 mm and 5 ml·min^{-1} as flow rate are assumed.

It can be seen that for any practical value of the coil diameter, the number of windings until the flow is developed is smaller than one. To introduce both chaotic fluid paths and radial mixing to the system, the number of windings is chosen to be two. As construction material, fluorinated ethylene propylene (FEP) was chosen because of excellent chemical resistance, mechanical flexibility and thermal stability [17] [18]. The inner diameter and length have been calculated according to the needed residence time and maximum pressure drop.
Other design parameters are coil diameter and pitch. The former needs to be maximized and the latter minimized in order to reduce torsion according to equation (5). Higher values for the helical flow group reduce the Dean vortex intensity. The design parameters of the investigated SHARCs can be found in Table 1.

Table 1: Design parameters for two SHARCs.

Parameter	Reactor A	Reactor B
d_i	0.75 mm	0.38 mm
d_a	1.59 mm	0.79 mm
D_{Coil}	20 mm	11 mm
h	7 mm	7 mm
l_R	6.25 m	6.25 m
$n_{winding}$	2	2
n_{Bends}	43	71

Coil arrangement

The target of the SHARC arrangement is to minimize space requirements. Additionally, a change of centrifugal force in four perpendicular spatial directions is desired to get the maximum possible reorientation of the axial flow profile, see Figure 1. Two different SHARC arrangements on a perforated metal plate were constructed, see Figure 3. The first setup A) is based on CFI structures by Nigam et al. [6]. A problem occurs by following a structure regularly in four spatially perpendicular directions such as in Figure 1; the in- and outlet of each 4-group of coils would need to go through exactly the same hole of the perforated plate. Hence, non-idealities in the structure are necessary. Two different compromises were implemented, which are displayed in Figure 4.

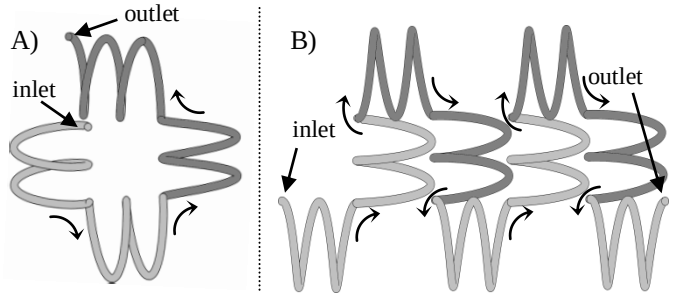

Figure 4: Different realized arrangements of the SHARC structures on perforated plates. A) shows the arrangement of Reactor A; B) of Reactor B.

In Figure 4A) the coil group at the top consists of 2.5 windings with the first 0.5 windings having a larger coil diameter. After every third bend such a modification to Reactor A has to be done. This is not necessary with a setup as shown in Figure 4B), but in this case the direction of the centrifugal force is only changed in three instead of four perpendicular directions. Because this influence on the RTD performance is unknown, it is currently studied by the Laboratory of Equipment Design. One advantage of this structure is its high spatial use. For that, multiple rows of the one shown above can be aligned in parallel. The light gray coils of this second row then would fit in between the dark gray ones of the first row. The realized structures are shown in Figure 3.

Temperature measurement

To characterize the SHARCs in terms of their heat transfer properties, type K thermocouples with a diameter of 0.25 mm were utilized. Since measurement of fluid temperature in a micro-scale environment always involves some disturbance in fluid flow, the temperature is measured at the outer tube surface. It is important that the measuring point is very to the

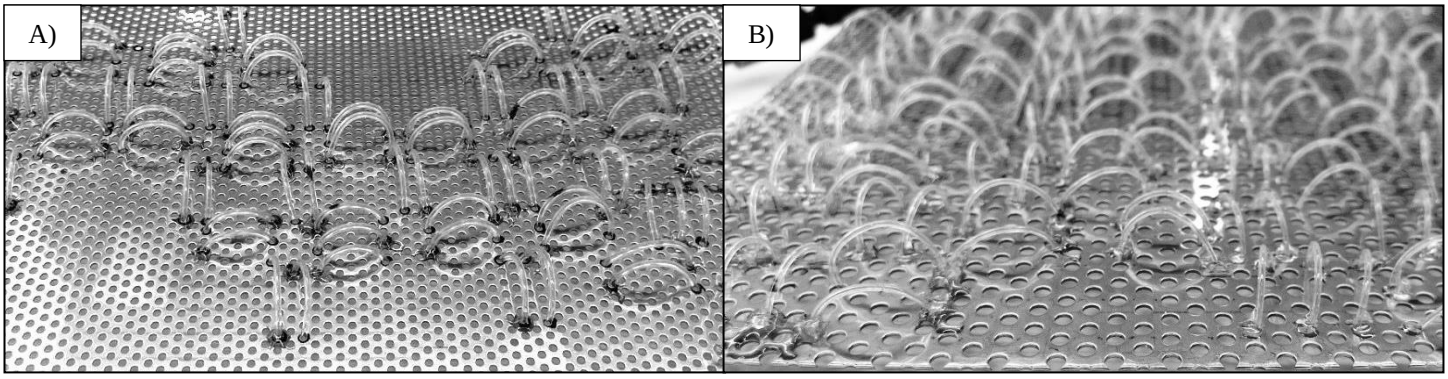

Figure 3: The two designed SHARCs on perforated plates with a hole diameter of 2 mm. The left and right pictures show Reactor A and Reactor B with 0.75 and 0.38 mm inner tube diameter, respectively.

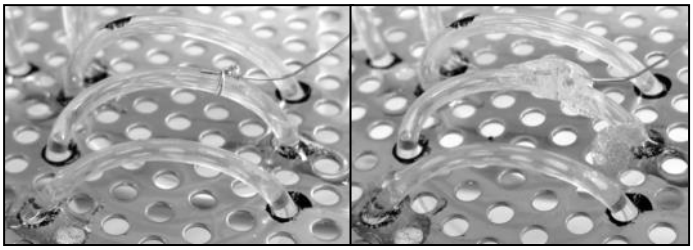

Figure 5: Attachment of the temperature sensor to the tube surface.

tubing surface, see Figure 5. On the left-hand side image in Figure 5, the temperature sensor has been fixed by twisting a metal wire around the tube so that the sensor position is as close to the surface as possible. On the right-hand side image, epoxy glue is used to secure both the sensor and the metal wire in the final position. Five to six temperature sensors were distributed over the reactor length for Reactor A and B, respectively.

EXPERIMENTAL

Residence time distribution RTD

From inlet to outlet of a chemical reactor not all fluid elements have the same velocity and do not leave the reactor after the same time. The particles leave in a more or less spread RTD. To characterize this behavior, the age distribution *E(t)* is used, which represents the probability of a particle to leave the reactor after a time *t*. To experimentally determine the age distribution, tracers are applied to the inlet of the reactor. When the tracer concentration is measured, the concentration distribution is equal to the age distribution. Its definition is shown in equation (10) [19].

$$E(t) = \frac{c(t)}{\int_0^\infty c(t)dt} \tag{10}$$

Due to disturbances in fluid flow, the measured age distribution function differs from ideal plug flow. A dispersion model regards non-idealities such as turbulent changes in flow velocity and vortices by a dispersion term. The representing parameter is the dimensionless Bodenstein number *Bo*, which is calculated by the flow velocity *u*, reactor length l_R and the axial dispersion coefficient D_{ax} from the dispersion model [20].

$$Bo = \frac{u \cdot l_R}{\mathrm{D}_{ax}} \tag{11}$$

If the Bodenstein number is relatively high (*Bo* > 100), the dimensionless age distribution function for an open system is close to plug flow behavior and can be represented by a Gaussian distribution with an error of less than 5% [21].

$$E(\theta) = \frac{1}{2}\sqrt{\frac{Bo}{\pi}}\,exp\left(-\frac{(1-\theta)^2 Bo}{4}\right) \tag{12}$$

For the experiments tracer pulse injections were conducted in a high pressure liquid chromatography (HPLC) from Agilent Technologies type 1220 Infinity LC. The chromatography column was substituted by the respective SHARC. As a tracer substance, 1mM sodium thiosulfate (TS) in aqueous solution is used as it shows a sharp absorption peak with a maximum at 230 nm [22]. Flow rates from 0.5 to 5.0 ml min^{-1} are investigated as the SHARC setup shows the most beneficial performance for low Reynolds numbers [7].
The reactor is fed with water at a constant flow rate. By using the auto-sample function of the HPLC, 5 µl of the 1 mM TS solution are injected. The response curve is then measured at the reactor outlet by UV-Vis spectroscopy. The integrated function of the Agilent Software is used to determine the area between response curve and the abscissa needed for equation (10).

Heat transfer

To characterize both SHARCs in terms of their heat exchange properties, the applied temperature sensors were used to measure heating and cooling profiles. When a differential heat balance is integrated and rearranged, the heat transfer coefficient can be calculated by measuring temperatures over the reactor length.

$$ln\left(\frac{T_{fluid}(z) - T_{cool}}{T_{inlet} - T_{cool}}\right) = -\left(\frac{\pi \cdot d_i \cdot k_{heat}}{\dot{m} \cdot c_P}\right) z \tag{13}$$

For a fixed flow rate and varying temperatures, the inner and outer heat transfer coefficients will be nearly constant. Only the heat transfer of the wall material will change. The heat capacity of the reactor material was found to be nearly constant for temperatures of 40 to 70 °C with a change of approximately 4.5% [23]. Thus, by choosing different coolant temperatures for each flow rate, nearly the same overall heat transfer should be obtained. This allows getting multiple data points for each flow rate.
The experimental setup for Reactor B is shown in Figure 6. For this SHARC, the heat transfer is measured in a water bath of a thermostat. The investigated flow rates are 3, 5 and 7 ml·min^{-1}, where for each flow rate heating profiles for four different coolant temperatures (40 to 70 °C) were recorded. HiTec Zang GmbH Syrdos2 syringe pumps are used to continuously feed de-ionized water through the reactor. Pressure and temperature data are collected with LabView, National Instruments.

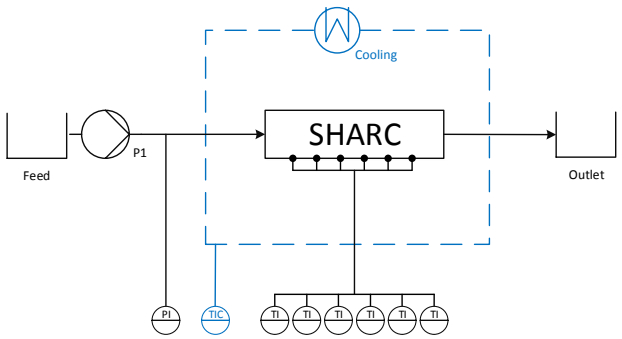

Figure 6: Flow sheet of the heat exchange experiments of Reactor B. Water at room temperature is pumped in the SHARC present in a tempered water bath.

For Reactor A the heat exchange to stagnant and convective air was investigated with a different plant setup. A preheater in a thermostat was used to set the inlet temperature to the desired value. The temperature was varied from 40 to 70 °C with feed flow rates of 5, 10 and 15 ml·min^{-1} for each temperature. From the heat exchanger, the fluid is fed into the SHARC, which was cooled at ambient temperature by either stagnant or convective air using a Clatronic HL 3378 fan heater. The heating function of this device was not utilized.

RESULTS

Residence time distribution

The response curves from the pulse injections are measured for flow velocities of 0.5 to 5 ml·min^{-1} and are shown in Figure 7.

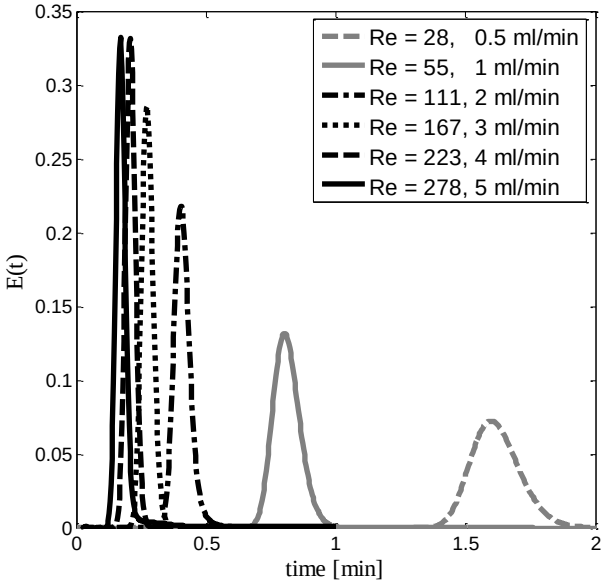

Figure 7: Measured age distribution curves for different flow rates over time. The SHARC with an inner diameter of 0.38 mm was used.

It can be seen that for lower flow rates, the RTD peak broadens and decreases in peak value. This is due to the fact that at low fluid particle velocity the tracers pass the sensor for a longer time. The area under each curve has to be constant for all experiments because the tracer concentration at 1 mM and the injected volume of 5 µl are constant. The peaks leave the reactor later for lower flow rates. MATLAB is used to minimize the sum of least squares of the difference between measured age distribution and Gaussian distribution curves by changing the Bodenstein number *Bo* in equation (12). The results of the fitted *Bo* number for both SHARCs and all experiments are shown in Figure 8. The *Bo* number is plotted against the Dean number *Dn* to take account of the different Dean vortex intensities.

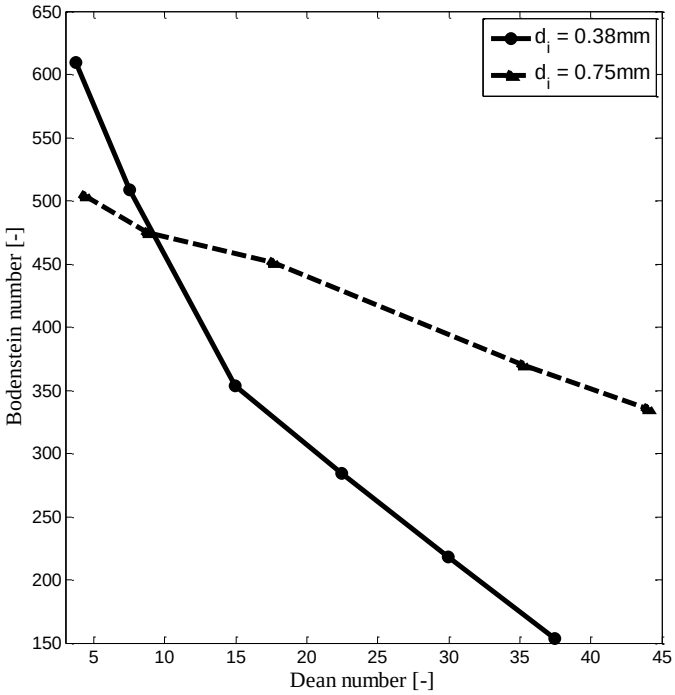

Figure 8: Bodenstein versus Dean number. The Bo number was calculated by the least squares fit to the measured dimensionless age distribution using a Gaussian distribution. Shown are the results for both SHARCs.

In comparison of both SHARCs, Reactor B shows a higher *Bo* number for low *Dn* numbers, while this trend is inversed for *Dn* numbers of about eight to ten. In this region, significant differences up to 230% between both reactors can be observed. As the *Dn* number already accounts for the inner diameter and the coil diameter, the only parameters, which can cause these differences, are torsion and the coil arrangement. The former is expected to have the major influence. Although the pitch distance with 7 mm is the same for both SHARCs, its influence on the Helical and Germano number (eq.(2)-(4)) increases for smaller coil and inner tube diameters. For the SHARC with an inner diameter of 0.38 mm the relative influence of the pitch is higher than for the one with 0.75 mm. Thus, former shows higher effects of torsion leading to higher axial dispersion. This is consistent with previous investigations about the effect of torsion [12]. The strong influence of the pitch on torsion is emphasized by the fact that Reactor B consists of 71 bends,

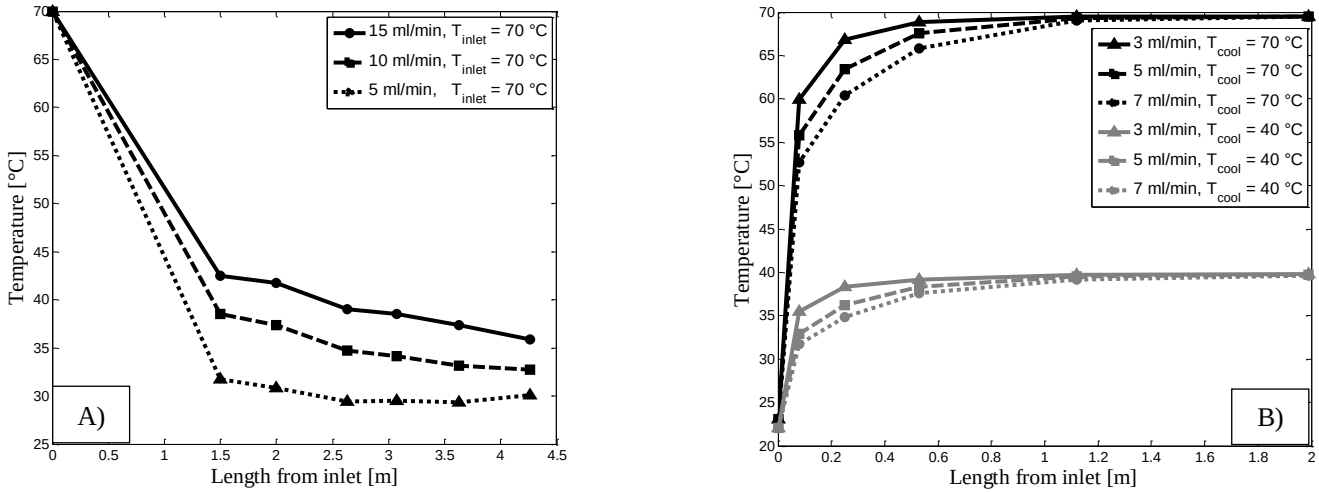

Figure 9: Measured temperature curves over the reactor length. A) shows a measured temperature profile of Reactor A with convective air cooling. B) shows the heating curves of Reactor B with water cooling for two different bath temperatures with three feed flow rated.

while Reactor A has 43. In literature it is always mentioned the number of bends has the highest impact on axial dispersion [7]. This has to be put into perspective for further reactor designs as minimizing the pitch is of high influence.

Heat transfer

A heating profile for convective air cooling and Reactor A is shown in Figure 9A). These experiments had a feed inlet temperature of 70 °C. It can be seen that the steepest decrease in temperature at the beginning of the reactor is not measured due to the temperature sensor distribution. This leads to flat temperature curves, which are more sensitive to disturbances. A higher flow rate causes a steeper profile and, hence, there is a higher temperature difference between each measuring point. A lower sensitivity to perturbations can occur.

The dotted temperature profile for a flow rate of 5 ml·min^{-1} is representative for errors in the temperature measurement. As the accuracy of the measuring box is limited to 0.3 °C, the temperature seems to rise for high reactor lengths, although it is expected to approach ambient temperature. The reason is the flat temperature profile and the inability of the sensors to indicate small changes over the reactor length.

For the water bath experiments of Reactor B in Figure 9B) the inlet temperature is assumed to be equal to ambient temperature. The process fluid was then heated to obtain the characteristic curves. For lower bath temperatures (gray lines), the fluid temperature approached the bath temperature at smaller entrance lengths due to smaller amount of heat to be transferred. The same trend was observed for smaller flow rates because of longer residence times. A highly stable temperature profile was measured with only small temperature fluctuations of the thermocouples.

The calculated heat transfer coefficients for Reactor A and air cooling are shown in Figure 11A). The solid lines represent least square fits. For stagnant air (gray squares) the heat transfer decreased with increasing flow rate. As the heat transfer is expected to be enhanced at higher flow rates, this indicates that the main heat transfer resistance is at the tube outside. Therefore, a change of the inlet flow rate has only a negligible influence on the heat transfer performance. All measurements indicate approximately the same heat transfer coefficients. The experiments were often disturbed by changes in ambient conditions as a completely non-convective environment cannot be achieved. The large error bar at a flow rate of 5 ml·min^{-1} appeared because a flat cooling curve was measured, which is more sensitive to small changes in temperature.

The trend for convective air cooling shows that the thermal resistance is still mainly on the outer tube side due to the low heat transfer coefficients; nevertheless, it is influenced by the feed flow rate. The experiments for the two lower flow rates show again higher relative errors because of a flat temperature profile. Volumetric heat transfer coefficients up to 0.432 MW/m³K were measured with a surface to volume ratio of 5333.3 m^{-1} (0.75 mm inner diameter).

Figure 11B) shows the calculated heat transfer coefficient for Reactor B (black circles). It can be seen that with higher flow rates the overall heat transfer increases. This is due to the fact that Dean vortex intensities increase, which lead to higher radial mixing and thus increased heat transfer. Despite the Dean vortices, a higher flow rate leads to a higher convective mass transfer, which also enhances the heat transfer. The standard deviation, which is indicated by the error bars, increases with increasing flow rate. For Reactor B and water cooling, volumetric heat transfer coefficients up to 7.55 MW/m³K were measured with a surface to volume ratio of 10526.3 m^{-1} (0.38 mm inner diameter).

Chemical reaction

With the reactor setup described before, the oxidation of thiosulfate (TS, $S_2O_3^{2-}$) by hydrogen peroxide (HP, H_2O_2) was carried out at various temperatures and concentrations at a fixed total feed flow rate of 5 ml·min^{-1}. With the thermocouples at the

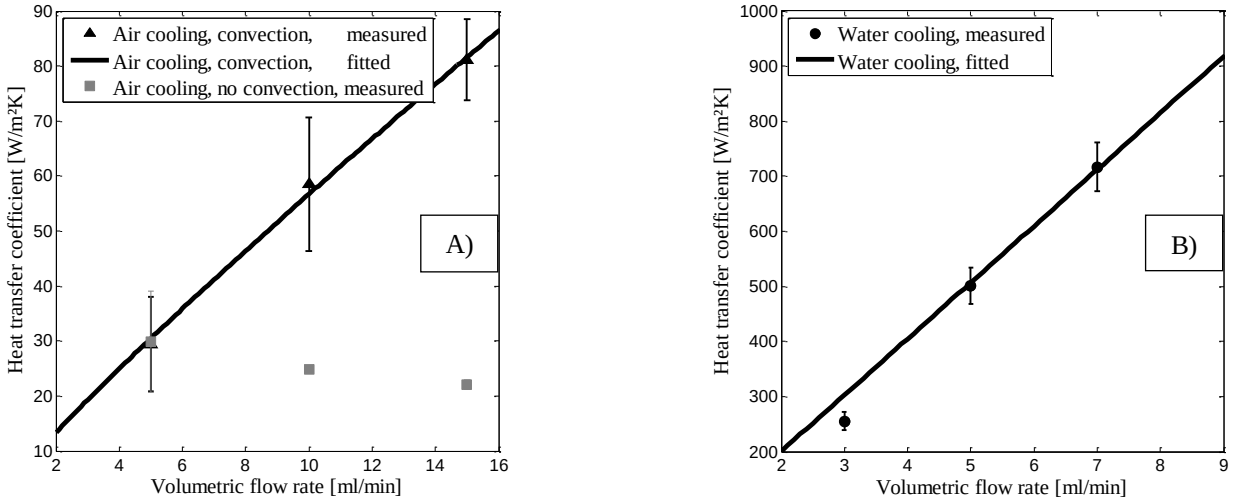

Figure 11: Measured overall heat transfer coefficients depending on the volumetric flow feed flow rate. The left figure shows the SHARC with d_i = 0.38 mm and water as a coolant. The right one displays d_i = 0.75 mm with convective (black triangles) and non-convective (grey squares) heat transfer to air. The bars indicate the standard deviation of the measurement, calculated from the deviation for the heat transfer coefficient for a fixed flow rate and variable inlet temperature. The solid lines represent fitted correlations with the least squares method.

tube outside the fluid temperature was measured during each run. The reactor was proven suitable to handle adiabatic temperature rises of more than 100 K due to its high heat transfer coefficient. A representative temperature profile can be seen in Figure 10.

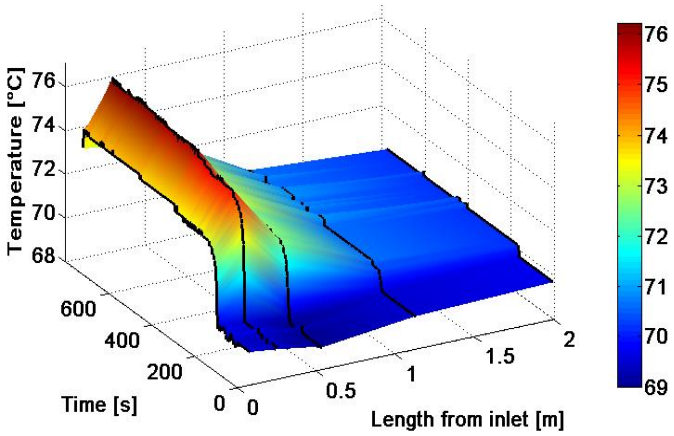

Figure 10: Temporal and local temperature distribution. T_{cool} = 70 °C, $c_{TS,0}$ = 0.337 mol·l^{-1}, $c_{HP,0}$ = 0.741 mol·l^{-1}, ΔT_{ad} =47.4 K.

At the beginning of the experiment, water is fed through the reactor to clean the tubes and adjust the temperature sensors. Accordingly, all sensors should measure the thermostat bath temperature. It can be seen in Figure 10 that, although the bath temperature as well as the reactor inlet temperature are expected to be the same at 70 °C, the thermocouples indicate lower values with deviations of about 1 °C. This is caused by the sensor accuracy. The relative error of the temperature measurement was determined to be smaller than 2%. After the feed streams are switched from water to the reagent solutions, it takes about 100 seconds for the reagents to reach the reactor inlet because of the tube length from the pumps to the T-shaped mixer. Water is substituted by the reagent and the reaction is initiated, indicated by the occurring hotspot. A sharp increase in temperature can be seen between sensor 1 and 2 (0.078 and 0.250 m from inlet, respectively). The profile is regarded as steady after seven minutes, at which only small temperature fluctuations are visible. However, small temperature deviations can be seen due to minor variations in flow rate combined with the deviations of the thermocouples. After about ten minutes the feed flow is stopped. The cooling is still sufficient to compensate the resulting decrease in heat transfer coefficient and no reaction runaway is present.

CONCLUSION

Two short helical alternating reactor capillaries (SHARC) were designed and constructed on perforated plates to achieve flexible designs with comparable geometries, even though irregularities in SHARC structures cannot be eliminated. The characteristic of this reactor is a compromise between chaotic fluid trajectories and radial mixing, which results in a high amount of bends for narrow residence time distribution RTD and high heat transfer coefficients.

The reactors were characterized in terms of heat transfer and RTD. Studying the latter it was found that Bodenstein numbers $Bo > 100$ can be achieved even though small Reynolds numbers ($14 < Re < 278$) were investigated indicating near plug flow behavior. In the design study the importance of torsion was shown by comparing two designed reactors. The influence of torsion can be higher than the number of bends, which was stated to be the main design parameter for the best SHARC performance [7]. This will be investigated in the near future.

The SHARCs were proven suitable for low Reynolds flow, which require a narrow RTD. The Dean vortices assure intense radial mixing and low axial dispersion. The SHARCs show high heat transfer coefficients and can be used for highly exothermic reactions. Especially polymerizations, which require high thermal control as well as low polydispersity indices can benefit for this setup.

For the test reaction of thiosulfate with hydrogen peroxide a stable continuous reactor operation was possible, even for high temperatures and concentrations. Due to high heat and mass transfer with volumetric heat transfer coefficients of up to 7.55 MW/m^3K, reaction runaway was prevented at high adiabatic temperature rises of more than 100 K.

NOMENCLATURE

Latin Letters:

Bo	Bodenstein number	[-]
c	concentration	[mol/m³]
c_P	heat capacity	[J/kgK]
D_{ax}	axial dispersion coefficient	[m²/s]
D_{coil}	coil diameter	[m]
d	diameter	[m]
Dn	Dean number	[-]
E	age distribution	[-]
Gn	Germano number	[1/m]
h	pitch	[m]
He	Helical number	[$m^{-0.5}$]
k_{heat}	heat transfer coefficient	[W/m²K]
l_R	reactor length	[m]
$\dot{m}$	mass flow rate	[kg/s]
$n_{winding}$	number of windings	[-]
Re	Reynolds number	[-]
Sc	Schmidt number	[-]
t	time	[s]
T	temperature	[K]
u	flow velocity	[m/s]
z	axial position	[m]

Greek Letters:

δ	curvature	[1/m]
ΔT_{ad}	adiabatic temperature rise	[K]
ς	helical flow group	[$m^{-0.25}$]
η_{coil}	torsion number	[1/m]
η	dynamic viscosity	[Pa·s]
θ	dimensionless time	[-]
ρ	density	[kg/m³]

Indexes:

0	inlet, initial condition
a	outer
cool	coolant
HP	hydrogen peroxide
i	inner
TS	sodium thiosulfate

ACKNOWLEDGMENTS

The authors thank Carsten Schrömges for laboratory assistance.

REFERENCES

[1] A. Varma, M. Morbidelli and H. Wu, Parametric sensitivity in chemical systems, Cambridge Univ. Press, 1999.

[2] W. Ehrfeld, V. Hessel and H. Löwe, Microreactors. New technology for modern chemistry, Wiley-VCH, Weinheim, 2001.

[3] D. W. Agar, S. Lohse, B. T. Kohnen, D. Janasek, P. S. Dittrich and J. Franzke, "A novel method for determining residence time distribution in intricately structured microreactors," *Lab Chip,* vol. 8, no. 3, p. p. 431, 2008.

[4] W. R. Dean, " XVI. Note on the motion of fluid in a curved pipe," *The London, Edinburgh, and Dublin Philosophical Magazine and Journal of Science,* vol. 4, no. 20, p. 208–223, 1927.

[5] K. D. P. Nigam and A. K. Saxena, "Axial dispersion in laminar flow of polymer solutions through coiled tubes," *J. Appl. Polym. Sci,* vol. 26, no. 10, pp. 3475-3486, 1981.

[6] K. Nigam, V. Kumar, M. Mridha and A. Gupta, "Coiled flow inverter as a heat exchanger," *Chemical Engineering Science,* vol. 62, no. 9, p. 2386–2396, 2007.

[7] K. D. P. Nigam, S. Vashisth and V. Kumar, "A Review on the Potential Applications of Curved Geometries in Process Industry," *Ind. Eng. Chem. Res* , vol. 47, no. 10, p. 3291–3337, 2008.

[8] K. D. P. Nigam, M. M. Mandal and P. Aggarwal, "Liquid-Liquid Mixing in Coiled Flow Inverter," *Ind. Eng. Chem. Res.,* vol. 50, no. 3, pp. 13230-13235, 2011.

[9] S. Liu and J. H. Masliyah, "Axially invariant laminar flow in helical pipes with a finite pitch," *J. Fluid Mech,* vol. 251 , no. 1, p. 315, 1993.

[10] K. Nigam and A. K. Saxena, "Coiled Configuration for Flow Inversion and Its Effect on Residence Time Distribution," *AIChE Journal,* vol. 30, p. 363–368, 1984.

[11] S. Litster, J. G. Pharoah and N. Djilali, "Convective mass transfer in helical pipes: effect of curvature and torsion," *Heat Mass Transfer,* vol. 42, no. 5, pp. 387-397, 2006.

[12] K. S. Kurt, Experimental Characterization of a New Virus Inactivation Method for Antibody Manufacturing, Master thesis, TU Dortmund University, Laboratory of Equipment Design, 2013.

[13] R. Trivedi and K. Vasudeva, "RTD for diffusion free laminar flow in helical coils," *Chemical Engineering Science,* vol. 29, no. 12, pp. 2291-2295, 1974.

[14] H.-U. Moritz, W. Schmidt, M. Ridder, C. Herrmann, W. Hübinger and J. Kremeskötter, "Vorrichtung zur kontinuierlichen Durchführung chemischer Reaktionen". Patent EP0944431, 1997.

[15] S. A. Berger, L. Talbot and L.-S. Yao, "Flow in Curved Pipes," *Annual Reviews of Fluid Mechanics* , vol. 15, no. 1, p. 461–512, 1983.

[16] L. R. Austin and J. D. Seader, "Entry Region for Steady Viscous Flow in Coiled Circular Pipes," *AIChE Journal*, vol. 20, no. 4, pp. 820-822, 1974.

[17] H. Domininghaus, Kunststoffe: Eigenschaften und Anwendungen, Springer, Berlin, 2011.

[18] Bürkle GmbH, "Chemische Beständigkeit von Kunststoffen," 29 07 2003. [Online]. Available: http://www.kuhnke.de/fileadmin/templates/content/Automation/Branchen/Medizintechnik/764343chemische_bestaendigkeit.pdf. [Accessed 28.03.2014].

[19] M. Baerns et al., Technische Chemie. Das Lehrbuch, Wiley-VCH, Weinheim, 2006.

[20] N. Kockmann, Transport phenomena in micro process engineering, Berlin: Springer , 2008.

[21] M. Kraume, Transportvorgänge in der Verfahrenstechnik, Springer, Berlin, 2012.

[22] C. Pan, Y. Liu, A. K. Horváth, Z. Wang, Y. Hu and C. Ji, "Kinetics and Mechanism of the Alkaline Decomposition of Hexathionate Ion," *J. Phys. Chem*, vol. 117, no. 14, p. 2924–2931, 2013.

[23] M. P. Data, "DuPont™ 100 FEP Fluorinated Ethylene Propylene," 2013. http://www.matweb.com/search/datasheet.aspx?matguid=3dbaaa8dbb114c57996acd6738a7efc1&ckck=1. [Accessed 28.03.2014].